In situ observation of reversible rippling in multi-walled boron nitride nanotubes

2011 Nanotechnology 22 115702

(http://iopscience.iop.org/0957-4484/22/11/115702)

Nanotechnology **22** (2011) 115702 (6pp) doi:10.1088/0957-4484/22/11/115702

In situ observation of reversible rippling in multi-walled boron nitride nanotubes

Hessam M Ghassemi[1], Chee H Lee[2], Yoke K Yap[2,3] and Reza S Yassar[1,3]

[1] Department of Mechanical Engineering-Engineering Mechanics, Michigan Technological University, 1400 Townsend Drive, Houghton, MI 49931, USA
[2] Department of Physics, Michigan Technological University, 1400 Townsend Drive, Houghton, MI 49931, USA

E-mail: ykyap@mtu.edu and reza@mtu.edu

Received 19 November 2010, in final form 13 January 2011
Published 4 February 2011
Online at stacks.iop.org/Nano/22/115702

Abstract

The recent observation of high flexibility in buckled boron nitride nanotubes (BNNTs) contradicts the pre-existing belief about BN nanotube brittleness due to the partially ionic character of bonding between the B and N atoms. However, the underlying mechanisms and relationships within the nanotube remained unexplored. This study reports for the first time the buckling mechanism in multi-walled BNNTs upon severe mechanical deformation. Individual BNNTs were deformed inside a transmission electron microscope (TEM) equipped with an *in situ* atomic force microscopy holder. High-resolution TEM images revealed that bent BNNTs form multiple rippling upon buckling. The critical strain to form the first ripple was measured as 4.1% and the buckling process was reversible up to 26% strain. As opposed to carbon nanotubes, the BNNTs buckled into V-shaped ripples rather than smooth wavy shapes. The rippling wavelength was quantified in terms of the outer diameter and thickness of the nanotubes. The BNNTs showed a larger rippling wavelength compared to that of CNTs with the same number of walls. This difference was explained by the tendency of BN structures to reduce the number of thermodynamically unfavorable B–B and N–N bonds at the sharp corners in the rippling regions. The BNNTs' structure also exhibited a higher fracture strain compared to their counterpart.

(Some figures in this article are in colour only in the electronic version)

List of symbols

λ	Buckling wavelength
ε	Strain
ν	Poisson ratio
h	Wavelength of buckling
r	Radius of nanotube
R	Radius of curvature

1. Introduction

The mechanical properties of boron nitride nanotubes (BNNTs) are measured and calculated both theoretically [1, 2] and experimentally [3, 4] to be in the same range as those of carbon nanotubes (CNTs), their structural analogue. However, they exhibit important advantages over CNTs, such as higher thermal/chemical stability [5] and thermal conductivity [6, 7]. In addition, their electronic properties are independent with respect to chirality, diameter, or nanotube length [8]. BNNTs offer a variety of applications in nano-scale electronic devices [9, 10], optoelectronics [11], and as a reinforcement in composites [12]. Despite the potential impact of BNNTs in many areas of science and industry, a robust understanding of their mechanical behavior is lacking and thus limits the design and optimization of BNNT-enhanced materials.

There are numerous reports on the mechanical responses of single- [13] and multi-walled CNTs [14–16], CNTs embedded in matrices [17, 18], or under torsion force [19]. Iijima *et al* [20] first observed single kinks in single-walled CNTs of diameters 0.8 and 1.2 nm bent to large angles.

[3] Authors to whom any correspondence should be addressed.

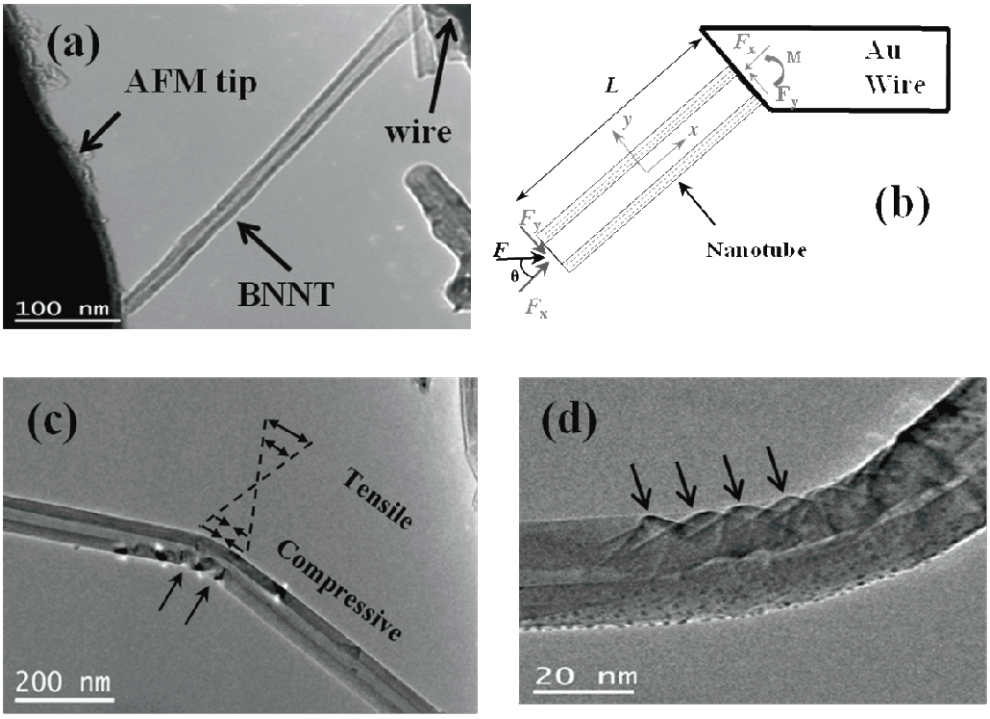

Figure 1. (a) Represents the bending experiment of an individual multi-walled BNNT in contact with an AFM tip (on the left) and a gold wire base (on the right). (b) Free-body diagram of the bending experiment in (a) with analysis of the associated forces. (c) The bent nanotube is shown and special pattern formation at the bent area is marked by arrows. (d) High-resolution (HR) TEM image of an individual bent BNNT reveals that the special pattern consists of multiple rippling on the compressive side of the nanotube.

Later on, they also reported that in the case of five-walled CNTs, first a single kink was developed; then at a higher bending curvature, the same nanotube developed double kinks. Transmission electron microscopy (TEM) images revealed that the distances between respective shells of the nanotube stayed unchanged, even in the presence of the kinks at high bending angles. Poncharal *et al* [16] and Bower *et al* [17] also observed local buckling of multi-walled CNTs during bending. Their TEM images indicate that the buckling wavelength is a function of the nanotube radius and wall thickness.

The authors recently reported [21] the mechanical characterization and fracture detection of individual BNNTs as a result of cyclic bending deformation. We observed the formation of several ripples during the bending deformation of multi-walled BNNTs. However, no quantitative correlation between the nanotubes' structural parameters and the rippling wavelength was given. Here, we examined the buckling formation of several BNNTs inside a TEM equipped with an atomic force microscope (AFM) and correlated the nanotube structural parameters and buckling characteristics.

2. Experimental procedure

The *in situ* experiments were conducted by an AFM that was operated inside a JEOL JEM-4000FX TEM at 200 kV. The BNNTs were directly deposited on Si substrates by thermal chemical vapor deposition at 1100–1200 °C in a conventional tube furnace [22]. Powders including MgO, Fe_2O_3, and pure B were used as precursors, and NH_3 gas was used as the source of nitrogen.

Individual BNNTs were then attached on an Au wire by light mechanical scratching on the as-grown samples. As a result of van der Waals forces, individual nanotubes stick to the wire in different directions. The Au wire was then fixed on the Au hat, which sits on the sapphire ball. Applying friction force between the hat legs and sapphire ball, the piezo-driven holder allows nanometer motion of the sample toward the AFM tip. The sample position can be adjusted with a precision of 1 nm in the X, Y and Z directions.

3. *In situ* bending experiments

Figure 1(a) shows a multi-walled BNNT between the AFM probe and the base of gold wire. At this initial stage, there is no sign of rippling throughout the length of the nanotube. Upon applying axial compressive force (F_x) on the nanotube, the nanotube starts to bend. The bending deformation is due to the moment M introduced as a result of the off-axis configuration between the nanotube and the support contacts. This is shown by the free-body diagram expression of the nanotube where the force, $\boldsymbol{F}$, is applied by the AFM tip along the horizontal direction (figure 1(b)). Assuming the two-dimensional coordinates along the nanotube axis, the force on the nanotube can be dissociated into F_x and F_y where $M = F_y L \cos\theta$, where L is the distance along the nanotubes axis between the contact points on the Au wire and the AFM tip, and θ is the angle between $\boldsymbol{F}$ and the nanotubes axis. Figure 1(c) shows multiple rippling formed around the bending center of the nanotube. The individual ripples are marked by

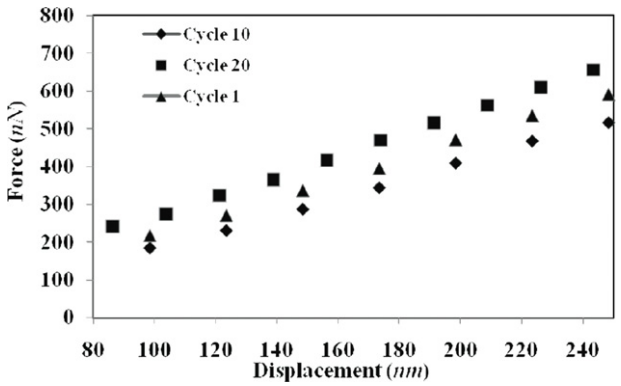

Figure 2. Force–displacement plots of a BNNT under cyclic bending deformation.

arrows in figure 1(d). The rippling formation was observed only on the compressive side of the nanotube and no sign of rippling was detected on the tensile part (figure 1(d)).

Figure 2 represents force–displacement plots of typical individual nanotubes under one, ten, and twenty cycles of bending deformation. Not much difference in terms of applied force at various cycles could be detected which suggests that the rippling formation is reversible. The HRTEM imaging of the nanotubes after unloading revealed no apparent fracture. Regularly distributed ripples were observed on the compressive side of the bent nanotube. Upon changing the direction of bending, the location of the buckles shifted. This, in fact, suggests that the buckle formation is reversible and is not affected by defects.

3.1. Buckling characteristics

During bending and buckling deformation, a distinct morphological characteristic for rippling was observed. The buckling was associated with sharp corners as shown in figure 3(a). The appearance of V-shape buckles has not been reported in CNTs [18, 14, 13]. The V-shaped ripple, shown in figure 3(a), has a folding angle of 120°. These sharp-cornered features are possible with the formation heptagon–pentagon pairs and unfavorable B–B or N–N bonds. The applied axial force, causing the bending deformation, can provide the energy required for this energetically unfavorable deformation. Hence, one can conclude that the nanotube transmits the applied deformation force through the above mentioned mechanism to avoid mechanical failure and maintain the nanotubular structure. This interpretation is consistent with the reported flat tip structure in BNNTs. Loiseau *et al* [23] described that such a flat tip structure corresponds to three interconnected hexagonal BN networks with 120° disclination in between. The results suggest that these thermodynamically unstable B–B/N–N bonds can switch back to stable B–N bonds as the force is unloaded, due to the more energetically favorite hexagonal BN structures. This conclusion is supported by the fact that multiple force–displacement data that were collected at various stages of rippling formation did not reveal obvious changes (figure 2).

The interlayer distances between the shells of the rippled area were not deviated from the original value of 0.35 nm, as shown in figure 3(a). This was validated by plotting the line intensity diagram of the nanotube (figure 3(b)) in the buckled area of figure 3(a). The existence of van der Waals forces between the B–N atomic layers can play a major role in controlling the inner shell distances. The importance of these forces was also reported by Cumings *et al* [24] during the telescoping phenomenon in multi-walled carbon nanotubes. The van der Waals forces between the B–N layers keep the inner shells' distance fixed, resulting in the rigid bending of B–N layers on top of each other. The van der Waals interactions also prevent the reduction of the inner diameter of the nanotube to below 0.35 nm, where these interaction forces become strongly repulsive. In other words, the van der Waals force can override the tube elasticity at *c*-axis.

3.2. Quantitative correlation of buckling and nanotube characteristics

Assuming zero strain along the axis of the nanotube, the off-axis/buckling strain (ε) can be calculated as r/R, where r is the radius of the nanotube and R is the radius of curvature measured at the hollow center of the nanotube. Measurements based on HRTEM images reveal that the first buckle starts to form at the ε range from 4.1–9%, depending on the wall thickness of nanotubes. This is in agreement with the results by Bower *et al* [17] where it is shown that the onset buckling strain of multi-walled CNTs inside a polymer matrix can reach up to 5%. The wall thickness represents the number of shells, which reflects the magnitude of B–N ionic bonds and also van der Waals force against the bending deformation. Upon further bending, the second buckle starts to form, mainly at $\varepsilon > 11.6\%$. Finally, at $\varepsilon \approx 26\%$, periodic ripples are formed next to each other, on the compression side of the nanotube. This level of strain is equivalent to 240 nm of displacement shown in figure 2. Upon unloading, the nanotube springs back to its original straight shape.

The circular cross section of the nanotube tends to be ovalized which is known as the Brazier effect [25]. The other mode of deformation in bending experiments is bifurcation, which is well known in continuum mechanics [26]. It is periodic rippling of the tube wall (figure 1(d)) that appears on the compressive stressed side of the nanotube. The wavelength of the rippling is predicted by Timoshenko's thin shell theory under axial compression as [27]:

$$\lambda = \frac{2\pi}{4\sqrt{12(1-\upsilon^2)}}\sqrt{rh} \tag{1}$$

where, υ is the Poisson ratio, r is the outer diameter and h is the wall thickness of the thin shell. Substituting the Poisson ratio of 0.2–0.4 [28] for *h*BNs, the value of $\lambda/\sqrt{rh}$ is found to be 3.4–3.5. In the case of nanotubes, the r, h, and λ parameters are shown in figure 4(a) and the variations of buckling wavelength for several BNNTs are plotted in terms of $(rh)^{0.5}$. The ratio $\lambda/\sqrt{rh}$ of multi-walled BNNTs is equal to ∼1.45, much smaller than the predicted value by classical mechanics (∼3.4). The difference can be explained by the

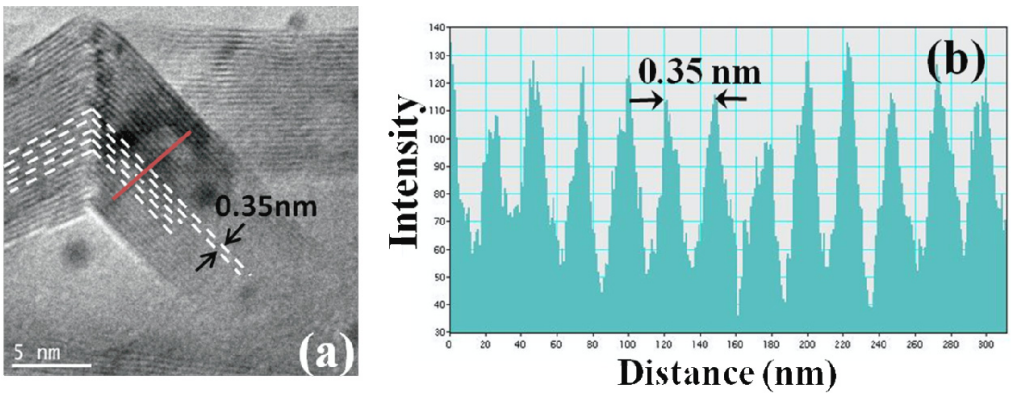

Figure 3. (a) HRTEM image of an individual BNNT shows typical V-shape buckles on the compression side. (b) The line intensity across along the red line in (a) indicates that the average distance between walls is ∼0.35 nm.

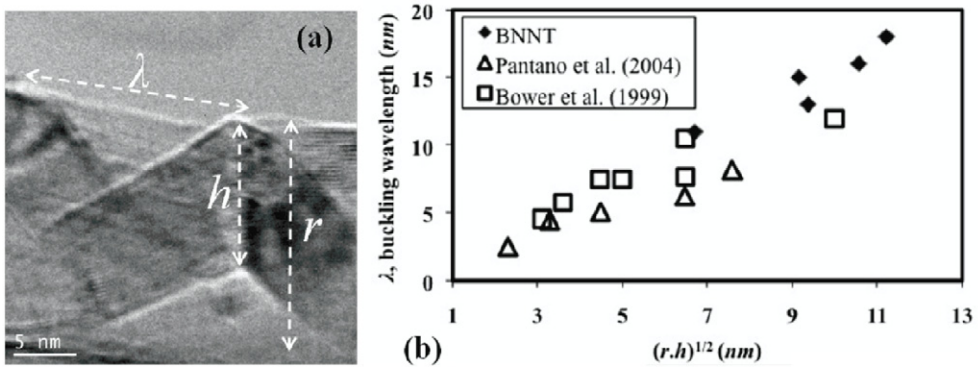

Figure 4. (a) Bright field TEM image of a buckled BNNT and the representative structural parameters r, h, λ and are shown. (b) The plot of buckling wavelength as a function of $(rh)^{0.5}$ where several BNNTs are compared with the available data on CNTs in the literature.

fact that the classical continuum mechanics models are defined for thin shell tubes where $r/h > 10$, while in multi-walled BNNT $1.3 < r/h < 1.8$. Moreover, in the case of nanotubes, the contribution of van der Waals interaction in transmitting the applied force through the shells should be taken into account. While, in classical continuum mechanics models the interaction between shells is ignored.

In figure 4(b), the data for buckling formation in BNNTs are compared with the similar phenomenon in CNTs reported by Bower *et al* [17] and Pantano *et al* [29]. In both cases of CNTs and BNNTs, as the thickness of nanotubes increase the wavelength of the buckles increases. However, in CNTs the ratio of $\lambda/(rh)^{0.5}$ is reported to be close to ∼1 [17], whereas we obtained the value of ∼1.45 for BNNTs. The reason for the higher rippling wavelength in BNNTs in comparison to that of CNTs can be explained in terms of minimization in the number of unfavorable B–B or N–N bonds. Figure 5(a) illustrates the hexagonal BN structure in each shell before bending deformation. The arrow indicates the bond switching that results in a heptagon–pentagon pair formation at the corner of the ripples as shown in figure 5(b). Hence, the system energy increases at those corners due to thermodynamically unfavorable B–B or N–N bonds, and thus the BN structure tends to minimize the number of B–B or N–N bonds. In contrast, in CNT structures, the C–C bonds have no thermodynamic restriction. Two hypothetical scenarios that can happen in the buckled BNNTs are described schematically in figure 5(c). In one scenario, two ripples with the wavelength of λ_1 are shown at a total length of $2\lambda_1$. Statistically this structure has three unfavorable B–B or N–N at the three sharp corners. In scenario two and for the same total length, the ripple with wavelength λ_2 has only two unfavorable B–B or N–N bonds. The latter scenario is more stable than the former and can explain the larger wavelength in BNNTs in comparison to CNTs.

4. Conclusion

Multi-walled BNNTs were subjected to buckling experiments inside a TEM. We observe that BNNTs are highly flexible which is counterintuitive knowing that they possess ionic structure. Multiple rippling was observed on the compressive side of the buckled nanotubes. The first ripple started at strain of 4.1%, and more ripples were formed by increasing the applied strain. Our results reveal that the rippling wavelength and nanotube outer diameter, r, and thickness, h, are correlated through the relationship of $\lambda/(rh)^{0.5} \cong 1.45$. It was also found that the buckling was reversible up to 26% strain. The buckling wavelengths in BNNTs are larger in comparison to

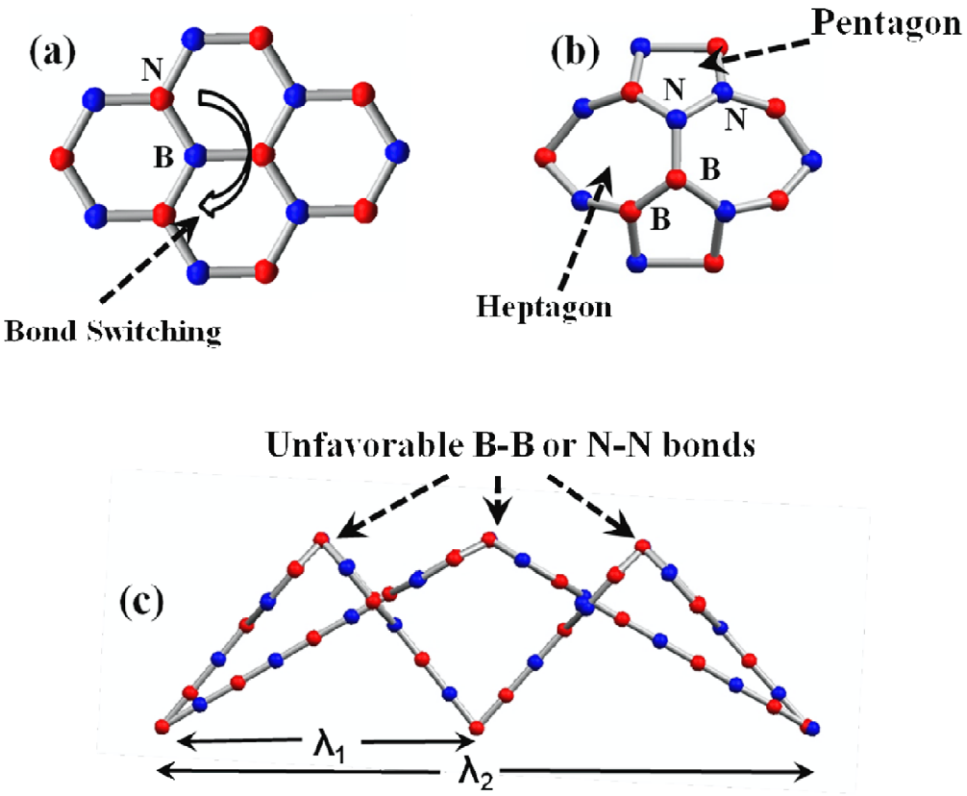

Figure 5. (a) Schematic of BN hexagon atomic arrangement in each shell before bending deformation. Arrow shows the direction of bond switching. (b) Top view of BN pentagon–heptagon pairs as a result of bending deformation. (c) A 2D schematic of ripples under two hypothetical scenarios. The ripples with wavelengths of λ_1 and $\lambda_2 = 2\lambda_1$ are shown for a total length of λ_2. Thermodynamically unfavorable B–B and N–N bonds are higher in the small ripples in comparison to the large ripple.

the data reported in the literature for CNTs. This difference was explained by the tendency of BN structures to reduce the number of unfavorable B–B and N–N bonds at the sharp corners in the rippling regions.

Acknowledgments

R S Yassar and Y K Yap acknowledge support from the National Science Foundation (Award No. 0820884, Division of Materials Research and Award No. 0926819, Civil, Mechanical and Manufacturing Innovation Division). Y K Yap acknowledges his National Science Foundation CAREER award (Award No. 0447555) and the US Department of Energy, the Office of Basic Energy Sciences (Grant No. DE-FG02-06ER46294) for supporting the efforts on the synthesis of boron nitride nanotubes.

References

[1] Verma V, Jindal V K and Dharamvir K 2007 Elastic moduli of a boron nitride nanotube *Nanotechnology* **18** 435711
[2] Song J, Huang Y, Jiang H, Hwang K C and Yu M F 2006 Deformation and bifurcation analysis of boron-nitride nanotubes *Int. J. Mech. Sci.* **48** 1197–207
[3] Suryavanshi A P, Yu M, Wen J, Tang C and Bando Y 2004 Elastic modulus and resonance behavior of boron nitride nanotubes *Appl. Phys. Lett.* **84** 2527–9
[4] Chopra N G and Zettl A 1998 Measurement of the elastic modulus of a multi-wall boron nitride nanotube *Solid State Commun.* **105** 297–300
[5] Golberg D, Bando Y, Kurashima K and Sato T 2001 Synthesis and characterization of ropes made of BN multiwalled nanotubes *Scr. Mater.* **44** 1561–5
[6] Xiao Y, Yan X H, Cao J X, Ding J W, Mao Y L and Xiang J 2004 Specific heat and quantized thermal conductance of single-walled boron nitride nanotubes *Phys. Rev.* B **69** 205415
[7] Tang C C, Bando Y, Liu C H, Fan S S, Zhang J, Ding X X and Golberg D 2006 Thermal conductivity of nanostructured boron nitride materials *J. Phys. Chem.* B **110** 10354–7
[8] Blasé X, Rubio A, Louie S G and Cohen M L 1994 Stability and band gap constancy of boron nitride nanotubes *Eur. Lett.* **28** 335–40
[9] Chico L, Crespi V H, Benedict L X, Louie S G and Cohen M L 1996 Pure carbon nanoscale devices: nanotube heterojunctions *Phys. Lett. Rev.* **76** 971–4
[10] Collins P G, Bando H and Zettl A 1998 Nanoscale electronic devices on carbon nanotubes *Nanotechnolgy* **9** 153–7
[11] Chen Z G, Zou J, Liu G, Li F, Cheng H M, Sekiguchi T, Gu M, Yao X D, Wang L h and Lu G Q 2009 Long wavelength emissions of periodic yard-glass shaped boron nitride nanotubes *Appl. Phys. Lett.* **94** 023105
[12] Hu N, Karube Y, Yan C, Masuda Z and Fukunaga H 2008 Tunneling effect in a polymer/carbon nanotube nanocomposite strain sensor *Acta Mater.* **56** 2929–36
[13] Yakobson B I, Brabec C J and Bernholc J 1996 Nanomechanics of carbon tubes: instabilities beyond linear response *Phys. Rev. Lett.* **76** 2511–4

[14] Kuzumakti T, Ayashih T, Ichinosek H, Miyazawka K, Ito K and Ishida Y 1998 *In situ* observed deformation of carbon nanotubes *Phil. Mag.* A **7** 1461–9
[15] Falvo M R, Clary G J, Taylor R M, Chi V, Brooks F P, Washburn S and Superfine R 1997 Bending and buckling of carbon nanotubes under large strain *Nature* **389** 582–4
[16] Poncharal P, Wang Z L, Ugarte D and Heer W A 1999 Electrostatic deflections and electromechanical resonances of carbon nanotubes *Science* **283** 1513–6
[17] Bower C, Rosen R, Jin L, Han J and Zhou O 1999 Deformation of carbon nanotubes in nanotube–polymer composites *Appl. Phys. Lett.* **74** 3317–9
[18] Lourie O, Cox D M and Wagner H D 1998 Buckling and collapse of embedded carbon nanotubes *Phys. Rev. Lett.* **81** 1638–41
[19] Jeong B W and Sinnott S B 2010 Unique buckling responses of multi-walled carbon nanotubes incorporated as torsion springs *Carbon* **48** 1697–701
[20] Iijima S, Brabec C, Maiti A and Bernholc J 1996 Structural flexibility of carbon nanotubes *J. Chem. Phys.* **104** 2089–92
[21] Ghassemi H M, Lee C H, Yap Y K and Yassar R S 2010 Real-time fracture detection of individual boron nitride nanotubes in severe cyclic deformation processes *J. Appl. Phys.* **108** 024314
[22] Lee C H, Wang J, Kayatsha V K, Huang J Y and Yap Y K 2008 Effective growth of boron nitride nanotubes by thermal chemical vapor deposition *Nanotechnology* **19** 455605
[23] Loiseau A, Willaime F, Demoncy N, Hug G and Pascard H 1996 Boron nitride nanotubes with reduced numbers of layers synthesized by arc discharge *Phys. Rev. Lett.* **76** 4737–40
[24] Cumings J and Zettl A 2000 Low-friction nanoscale ninear bearing realized from multiwall carbon nanotubes *Science* **289** 602–4
[25] Ju G T and Kyriakides S 1992 Bifurcation and localization instabilities in cylindrical shells under bending II Predictions *Int. J. Solids Struct.* **29** 1143–71
[26] Landau L D and Lifshitz E M 1986 *Theory of Elasticity* (Oxford: Pergamon)
[27] Timoshenko S 1936 *Theory of Elastic Stability* (New York: McGraw-Hill)
[28] Cardinale G F, Howitt D G, McCarty K F, Medlin D L, Mirkarimi P B and Moody N R 1996 Analysis of residual stress in cubic boron nitride thin films usingmicromachined cantilever beams *Diamond Relat. Mater.* **5** 1295–302
[29] Pantano A, Parks D M and Boyce M C 2004 Mechanics of deformation of single- and multi-wall carbon nanotubes *J. Mech. Phys. Solids* **52** 789–821